DENSITY AND SP^3 CONTENT IN DIAMOND-LIKE CARBON FILMS BY X-RAY REFLECTIVITY AND ELECTRON ENERGY LOSS SPECTROSCOPY

A. LIBASSI[1], A. C. FERRARI[2], V. STOLOJAN[3], B. K. TANNER[1], J. ROBERTSON[2], L. M. BROWN[3]
[1]Department of Physics, University of Durham, Durham, DH1 3LE, UK
[2]Department of Engineering, University of Cambridge, Cambridge, CB2 1PZ, UK
[3]Cavendish Laboratories, University of Cambridge, Cambridge CB3 OHE, UK

ABSTRACT

Grazing angle x-ray reflectivity (XRR) is used to study density, thickness, internal layering and roughness of a variety of carbon samples, with and without hydrogen and nitrogen. The bulk mass density of optimised tetrahedral amorphous carbon (ta-C) is 3.26 g/cm^2, for which Electron Energy Loss Spectroscopy (EELS) found a sp^3 fraction of 85%. Combining XRR and EELS we benchmark the dependence of sp^3 fraction on density for hydrogen-free carbons. Hydrogenated ta-C (ta-C:H) deposited by electron cyclotron wave resonance (ECWR) reactor from acetylene gas, has a density of 2.35 g/cm^3, 75% sp^3 and ~30% hydrogen. These data provide a similar validation for density and sp^3 EELS data for hydrogenated DLCs. XRR can also reveal internal layering in films, and indeed less dense layers may be found at the surface or interface of ta-C films, but no such layers are found in ta-C:H films.

INTRODUCTION

Density, sp^3 fraction, clustering of the sp^2 phase, hydrogen content and internal layering are the important structural parameters that determine the properties of amorphous carbons. Electron Energy Loss Spectroscopy (EELS) is presently the method of choice for sp^3 measurements, from the size of the π^* peak in the carbon K edge absorption spectrum, and the mass density can be deduced from the valence plasmon energy. Here, we show how grazing incidence x-ray Reflectivity (XRR) can be used to obtain information about density, roughness and cross-sectional layering for any amorphous carbon, without any sample preparation or damage [1-5]. Information about the possible layering within the films. This could be obtained by cross sectional EELS, but only with complex and careful sample preparation [6].

XRR gives information about the total electron density, which can be directly translated into mass density [5]. On the other hand, density determinations via EELS rely on an effective electron mass, for which different values can be found in literature [7-9]. We will show how a correct fit of the plasmon peak and an appropriate choice of the effective mass can give good agreement with the XRR mean densities, thus validating the use of the quasi-free electron model to analyse the low loss spectrum. Indeed an unique effective mass for all amorphous carbons and diamond is obtained.

EXPERIMENTAL
Samples

We analysed tetrahedral amorphous carbon, ta-C, hydrogenated ta-C, ta-C:H, nitrogen containing ta-C:H, amorphous carbon (hydrogenated) a-C: (H), and nanostructured a-C, all deposited on Si. Two sets of ta-C films were analysed. The first was deposited using a single

bend Filtered Cathodic Vacuum arc (FCVA) system [8] with different biases. The second series of ta-C films was deposited at different bias on a S-Bend FCVA [10]. Two series of ta-C:H samples were obtained using an Electron Cyclotron Wave Resonance source with an acetylene plasma and an ion energy from 80 to 170 eV [11]. Elastic Recoil Detection Analysis (ERDA) gave ~30% at. H for all the films. One ta-C:H was deposited from methane with a Plasma Beam Source [12] with~40% at. H. Three ta-C:H:N were deposited by an ECWR source from N_2/C_2H_2, with known C/N and C/H ratios, by ERDA-XPS [11]. Three a-C:H were deposited from methane using a PECVD, two diamond like with an estimated H content ~30-40% at. and one polymeric a-C:H with an estimated H~40-50%at. An a-C sample deposited by DC magnetron sputtering and a nanostructured a-C film was deposited by a pulsed microplasma cluster source [13].

XRR and EELS

Specular reflectivity curves were acquired with a Bede Scientific GIXR reflectometer, with a Bede EDRa scintillation detector, using the Cu K_β radiation (λ=1.3926 Å). Specular and off-specular reflectivity curves were measured for each sample, with the incidence angle θ_i in the range 0-8000 arcsecs, with a step of 20 arcsecs. Simulations were performed using the Bede REFS-MERCURY software package, which uses Parrat's recursive formalism of the Fresnel equations to calculate the reflected wave amplitude and, hence, the reflected intensity [5, 14-16]. XRR probes atomic scale surface roughness which results in x-rays being scattered out of the specular beam, causing a reduction in the specular reflected intensity. The intensity fall is faster than $(2\theta)^{-4}$, which holds for a perfectly smooth surface. By combining specular and diffuse scatter, genuine surface roughness can be separated from compositional grading [15]. XRR probes a macroscopic area of the sample (~cm^2).

EELS measurements were carried out on a VG 501 Scanning Transmission Electron Microscope (STEM) with a McMullan parallel EELS detection system [17]. The carbon K edge and the valence loss spectra were acquired for each sample at convergence semi-angle of 7.4 mrad and collection semi-angle of ~7mrad. This ensures that the sp^2 bonds are counted independently of their orientation [20]. The standard analysis [8,18,19] was then employed to obtain the single-scattering K-edge and plasmon peak respectively. The π^* peak in the carbon K-edge was modeled with a gaussian, and its area was normalised to the experimental spectra. Referring this to graphite, the sp^2 content is obtained [8, 19, 20], with 5% error. The plasmon energy results from fitting the quasi-free electron model to the plasmon peak.

RESULTS
X ray Reflectivity

The refractive index for x-rays in solids is smaller than unity, so that total external reflection occurs at low angles of incidence. As the incidence angle θ_i increases above a critical angle θ_c, x-rays start to penetrate into the film. From Snell's law at the air/film interface, one can obtain the critical angle for a medium with 3 elements, Carbon Nitrogen and Hydrogen:

$$\theta_c = \lambda \sqrt{\frac{N_A r_0}{\pi} \rho \frac{[X_C(Z_C + f_C') + X_H(Z_H + f_H') + X_N(Z_N + f_N')]}{(X_C M_C + X_H M_H + X_N M_N)}} \qquad (1)$$

where $r_0 = e^2/4\pi\varepsilon_0 m_e c^2$ is the classical electron radius, N_A is the Avogadro number, M_C, M_H and M_N are the carbon, nitrogen and hydrogen molar masses, f_j' takes dispersive corrections

into account; ρ is the mass density and X_j is the atomic fraction. At $\lambda=1.3926$ Å, $f_i' \sim 10^{-2}$. Thus assuming $f_j' = 0$, we obtain, with $X_H=1-X_C-X_N$:

$$\rho = \frac{\pi^2 c^2 \varepsilon_0}{3\lambda^2 N_A e^2} M_c m_e \theta_c^2 \frac{11X_C + 13X_N + 1}{5X_C + 6X_N + 1} \qquad (2)$$

We note that the dependence on the H content is quite small in the usual range $X_H = 10\text{-}50\%$.
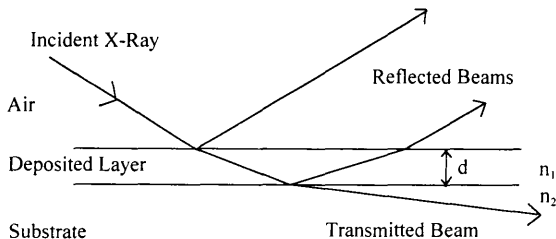
Fig.1: Reflection of x-rays under grazing incidence from a single layer of refractive index n_1 and thickness d on a substrate of refractive index n_2.

For a thin layer on a substrate (Fig.1) the two rays reflected at the film surface and at the film-substrate interface can interfere. From Snell's law, we have constructive interference when:

$$\theta_r^2 = \theta_c^2 + \frac{\lambda^2}{4d^2}(k+1/2)^2 \qquad \text{when } n_1 < n_2 \qquad (3a)$$

or

$$\theta_r^2 = \theta_c^2 + \frac{\lambda^2}{4d^2}k^2 \qquad \text{when } n_1 > n_2 \qquad (3b)$$

where d is the thickness and k is an integer. For $\theta_r > 2\theta_c$ the spacing between the fringes is $\Delta\theta \cong \lambda / 2d$. Thickness can thus be found from the fringe period [14].

For films with low density, a double critical angle is clearly distinguishable thus allowing an easier determination of the density (Fig.2). For ta-C:H only one fringe period is seen, indicating that these films consist of a single layer. The presence of a ~1-2 nm layer of different density (possibly composed of Si, C, O [2, 6]) at the film-substrate interface gives an even better fit. Ta-C:H films have a density in the range 2.1-2.4 g/cm³. A similar behaviour was obtained for a-C:H films, but with a clear double critical angle structure, giving a density of 1.64-1.74 g/cm³ for diamond-like samples and 1.2 g/cm³ for the polymeric one (Fig 3a). The ta-C:H:N in Fig 3a showed a total thickness of 95nm, and a density of 1.8 g/cm⁻², with less than 2nm Si/C and Si/air interfaces.

For ta-C films, it is easier to determine the film density, as the critical angle is greater than the Si critical angle. Densities up to 3.26 g/cm³ were obtained for an 88% sp³ film from the S-Bend FCVA. However, for the single bend FCVA, the reflectivity curves show multiple periodicities, which indicate internal layering. They can be reproduced only by taking into account two or more layers with different densities. In general, if a film consists of a bulk, dense layer and thinner and less dense layers at the top and the bottom, the critical angle is that of the bulk layer. Thus, from the critical angle, we directly get the density of the densest layer and not the average film density, which requires a fit of the multilayer structure. The film grown at -80 V shows a smaller period corresponding to the overall film thickness and a bigger period corresponding to a less dense surface layer ~7nm thick (Fig. 3a). Other films

show more complex curves (Fig 3b). The number of layers, their density, thickness and roughness are all variable and the density of the top and bottom layers (and maybe of the bulk)
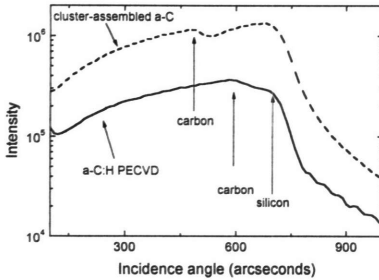
Fig.2: Double critical angle in the cluster-assembled carbon film and in an a-C:H film
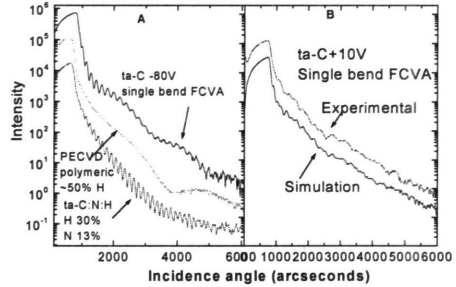
Fig.3a: Reflectivity curve of the single bend FCVA ta-C −80 V; PECVD a-C:H polymeric film (~50%H); ta-C:H:N film (30% H, 13% N)

Fig.3b: Reflectivity curve of the ta-C +10 V film; the bottom line, shifted for clarity, is a simulation of a film with 3 layers of density 2.56, 2.72 and 2.43 g/cm^{-2} and thickness 27.5, 37 and 9 nm

is probably not constant, whilst the sp^3 content does not vary so much with bias. Simulation of such a structure is difficult. The optimum −80V bias corresponds to the minimum thickness for the less dense layers. On the other hand, ta-C films grown with the S-bend filter show a much higher uniformity and only a slight dependence of density and layering on the substrate bias. Surface layers never exceed 1-2 nm. The thickest one, 2nm, is seen for the film grown at -300 V bias. The magnetron sputtered a-C shows a clear double critical angle, corresponding to ρ ~1.7 (±0.05) g/cm^3. The reflectivity curve exhibits 3 different periodicities, corresponding to ~360 nm (total thickness), ~40nm and ~5 nm (surface layers) with ρ varying from 1.7 to 1.15 g/cm^3 in the surface layer. A clear double critical angle structure was detected for the nanostructured a-C, resulting in densities of ~1 g/cm^3 to ~1.4 g/cm^3, depending on the size of the deposited clusters (Fig.2) [13].

The top surface r.m.s. roughness was found to be in the range 5-8 Å for all the films, and no direct relationship between roughness and deposition parameters could be found. Another set set of films was grown with a single bend FCVA at −80V with increasing deposition times (from 20 to 90 secs). In this case particular care was taken in minimising the plasma instabilities. XRR showed an increase in thickness without the development of any surface layer. The roughness increased from 4-5 Å to 9-10Å. This indicates that very uniform ta-C films can be grown even with the single bend FCVA, at least at −80V.

EELS

The low energy loss spectrum is proportional to the energy loss function, which can be described, in the framework of the Jellium model and small scattering vector, as [18]:

$$\mathrm{Im}\left[\frac{-1}{\varepsilon(E)}\right] = \frac{E(\Delta E_p)E^2{}_p}{(E^2 - E^2{}_p)^2 + (E\Delta E_p)^2} \qquad (4)$$

where ε(E) is the dielectric function, E$_p$ is the plasmon energy and ΔE$_p$ is the FWHM of the energy loss function. The plasmon energy is defined as:

$$E_p = \hbar \left(\frac{ne^2}{\varepsilon_0 m^*} \right)^{\frac{1}{2}} \qquad (5)$$

To derive the mass density from the valence electron density, we assume that C contributes 4 valence electrons N contributes 5 electrons and H contributes 1 electron, obtaining:

$$\rho = \frac{\varepsilon_0}{12\hbar^2 N_A} M_C m^* E^2_P \left(\frac{11X_C + 13X_N + 1}{3X_C + 4X_N + 1} \right) \qquad (6)$$

The structure of eq (2) and (6), giving the mass density via XRR and EELS, can be directly compared. In (2) the unknown parameters are the critical angle, θ_c, the carbon fraction, X_C, and nitrogen fraction X_N, whilst m_e is the free electron mass. In (6) the unknowns are the plasmon energy, E_P, the carbon fraction X_C, the nitrogen fraction X_N and the electron effective mass, m^*. Eq (2) has a weaker dependence on the H content. Approximations used to get (6) are cruder than the ones for (2). Moreover, $4X_N$ in (6) arises from the assumption of 5 valence electrons given by N. The weaker point of (6) is the unknown electron effective mass which naturally arises from the assumption of a quasi-free electron model. The usual approach is to derive m^* in (6) so that the density of diamond (3.515 g/cm^3) corresponds to its plasmon energy of 33.8 eV [8]. This gives $m^* \sim 0.85 m_e$. However, some groups assumed $m^* = m_e$, thus considering the electrons totally free [9], introducing a ~15% difference in the calculated densities. Weiler et al.[21] proposed a common sp^3-density relationship for ta-C and ta-C:H. Closer inspection of the original data reveal that a different electron mass was used by Fallon et al [8] and Weiler [21], resulting in a ~15% overestimation of the density of ta-C:H. Our data from XRR on similar ta-C:H films indicate a maximum density of 2.39 g/cm^3 comparable with the ~2.4 g/cm^3 obtained on scaling by 15% the original data of Weiler.
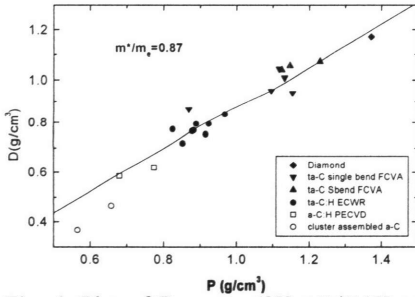
Fig. 4: Plot of D = $\rho_{XRR}(3X_C+1)/(11X_C+1)$ in function of P= $m_e M_C \varepsilon_0 (12 \, \hbar^2 \, N_A)^{-1} E_P^2$. The slope of the linear fit is m_e/m^*.
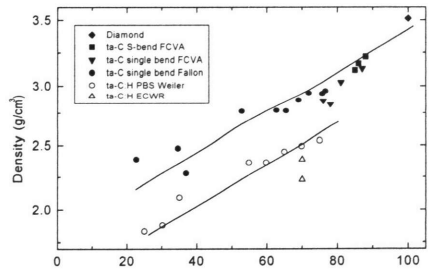
Fig 5: Variation of sp^3 fraction and density for ta-C and ta-C:H films. The lines are guide to the eye

XRR should be the method of choice to measure the mass density. Not only it is superior to the plasmon energy approach, but also to other approaches such as floating measurements and RBS plus profilometry. Yet, EELS remains still the standard choice of measurement of the sp^3 fraction, obtaining the plasmon energy at the same time. Using the independent mass determination from XRR, we can fit an effective electron mass that can be used to get a rough estimate of the density from the plasmon energy of all amorphous carbons. Thus, from (6), we plot in Fig. 4 the reduced densities from XRR and EELS, D=$\rho_{XRR}(3X_C+1)/(11X_C+1)$ against P =$m_e M_C \varepsilon_0 (12 \, \hbar^2 \, N_A)^{-1} E_P^2$, to obtain a line with slope m^*/m_e= 0.87. Only samples with X_N=0 were considered. This is a direct evidence of the existence of a common effective mass for diamond and all amorphous carbons. Indeed, this

gives E_p (diamond) ~33.4 eV, within the 0.5eV experimental error. We can now give a relation between sp^3 and density, as shown in Fig 5, where the data are scaled with our fitted m*. For ta-C:H:N samples a good agreement with XRR was obtained using our fitted m* and 5 valence electrons, thus confirming the validity of eq. (6)

CONCLUSIONS

A wide variety of amorphous carbons have been analysed via XRR and EELS. XRR is shown to be the method of choice to measure their density and cross-sectional structure. Comparing XRR and EELS data we fitted a common effective electron mass for all amorphous carbons and diamond. We have thus shown a general relationship between sp^3 and mass density for ta-C and ta-C:H. The cross-sectional structure of hydrogenated films is found to be quite uniform, with less than 1-2 nm interface and eventually surface layers. Ta-C can possess a heavily layered structure depending on the deposition conditions. Our S-bend FCVA is found to give the most uniform ta-C films. Heavy layering is thus linked to the particular deposition system and is not a fundamental property of ta-Cs. Plasmon energy is convenient to get the average density of heavily layered films when fitting of XRR data is difficult.

ACKNOWLEDGEMENTS

REFERENCES

1. F. Toney and S. Brennan, J. Appl. Phys. **66**, 1861 (1989)
2. A. Lucas, T. D. Nguyen and J. B. Kortright, Appl. Phys. Lett. **59**, 2100 (1991)
3. S. Logothetidis, G. Stergioudis, Appl. Phys. Lett., **71**, 2463 (1997)
4. Q. Zhang, S. F. Yoon, Rusli, J. Ahn, H. Yang and D. Bahr, J. Appl. Phys. **86**, 289 (1999)
5. B. Lengeler, *X-ray Absorption and Reflection in the Hard X-Ray Range*, ed. by M. Campagna and K.Rosei, North Holland (1990)
6. C. A. Davis, K. M. Knowles and G. A. J. Amaratunga, Phys. Rev. Lett. **80**, 3280 (1998)
7. D. R. McKenzie, D. Muller and B. A. Pailthorpe, Phys. Rev. Lett **67**, 773 (1991)
8. P. J. Fallon, et al., Phys. Rev. B **48**, 4777 (1993).
9. R. Lossy et al. , J. Appl. Phys., **77**, 4750 (1995)
10.M.C. Polo, J. L. Andujar, A. Hart, J. Robertson, W.I. Milne, Diamond Relat. Mats,(1999).
11.S. E. Rodil, N. A. Morrison, J. Robertson, W. I. Milne, Phys. Stat. Sol A, **337**, 71 (1999)
12.N. M. J. Conway et al., Appl. Phys. Lett. **73**, 2456 (1998).
13.P. Milani, et al., J. Appl. Phys. **82**, 5793 (1997).
14. L. G. Parrat , Phys. Rev. **95**, 359 (1954)
15. M. Wormington et al., Phil. Mag. Lett., **74**, 211 (1996).
16. S. K. Sinha, E.N. Sirota, S. Garoff, Phys. Rev. B **38**, 2297 (1988)
17. D. McMullan, P. J. Fallon, J. Ito and A. J. McGibbon, *Electron Microscopy*, vol 1, EUREM 92, Granada, Spain, p.103, (1992)
18.R. F. Egerton, *Electron Energy Loss Spectroscopy in the Electron Microscope*, Plenum, New York (1996)
19.S. D. Berger, D. R. McKenzie and P. J. Martin, Phil. Mag. Lett. **57**, 285 (1988)
20. N. K. Menon and J. Yuan, Ultramicroscopy **74**, 83 (1998).
21. M. Weiler, et al. Phys. Rev. B, **53**, 1594 (1996).